Thin-bed AVO and AVF continued

Wenyong Pan, Kris Innanen

ABSTRACT

Zoeppritz equations are the basis for traditional AVO analysis, which plays a significant role in oil and gas exploration. While they are not suitable for quantitative analysis of the amplitude response of thin-bed. In this paper, we continued our research on thin-bed AVO analysis. Firstly, we review our method for thin-bed AVO analysis. And then we extend our analysis of thin-bed AVO with attenuation from a dispersion-free system to the dispersion system, which means that the amplitude response is frequency dependent. And we found that if the thin-bed thickness and Q are both fixed, with increasing frequency, the Real part of R_{PP} AVO curve departs that with no attenuation, while the Real part of R_{PS} AVO curve approaches that without attenuation. What's more, the influence of Q on Real parts of the reflections increases with thin-bed thinning. Then we tested a linear approximation analysis following Liu and Schmitt (2003)'s method. We concluded that with thin-bed thinning, the approximations approach the exact values better. Finally, we compared our method for thin-bed AVO analysis with the numerical modeling results. And the amplitudes calculated by our method match the numerical results very well, which also prove the correctness of our method.

THIN-BED AVO THEORY REVIEW

Amplitude Variation with Offset (AVO) technique is using the amplitude variations for hydrocarbon detection. And the basis for AVO technique is Zoeppritz equations and they describes the transmission and reflection when plane wave impinging upon one single interface which separates two infinite half spaces. The single interface model is shown in Fig.1. When a plane P-wave illuminates the single interface, the transmitted P and S wave and reflected P and S wave are produced. However, the Zoeppritz equations do not permit quantitative interpretation of the response of thin beds. As a geological layer thins, the reflections from the top and bottom interfaces overlap, and the resulting wave is significantly different from that due to a single interface.

Our geometrical configuration is illustrated in Figure 1: a three-layer model used in this research. The thin-bed (layer 2) is embedded between two infinite half spaces. A plane harmonic and compressional wave (P-wave) impinges on interface 1, causing both a reflected P-wave and a reflected (converted) shear wave (S-wave), as well as a transmitted P-wave and S-wave. The transmitted P-wave and S-wave produce multiple reflections within layer 2. The total wave response involves overlapping reflected and transmitted waves at point C in Figure 1. This renders the Zoeppritz equations unsuitable as a tool for analysis of the upgoing field due to interface 1. In Figure 1, z is the thickness of thin-bed (Layer 2). In this research, we use $n = \lambda/z$ to analyze the AVO responses when varying z, where λ is the dominant wavelength.

We simplify the layered elastic medium theory due to Brekhovskikh (1993), to coincide with three-layer elastic media. The displacements and stresses in layer 1 and layer 3 are connected by one coefficient matrix $\mathcal{C}$, as shown in equation (1). Each element in matrix $\mathcal{C}$
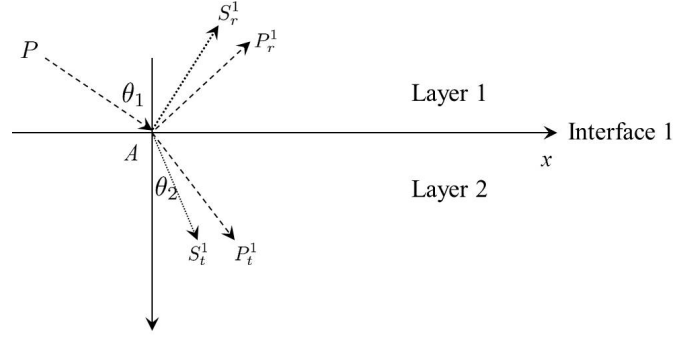
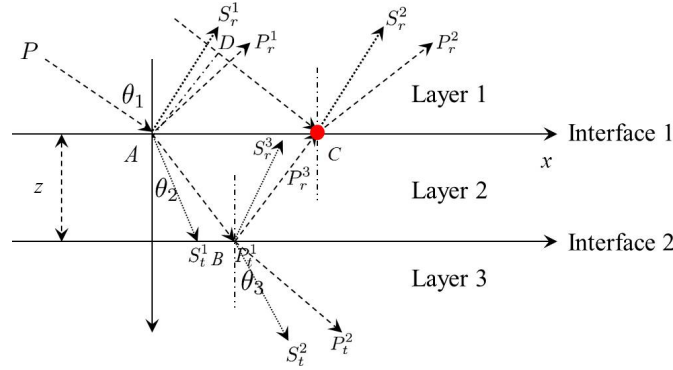FIG. 1. Single interface model for traditional AVO analysis.

FIG. 2. Three layer model for thin-bed AVO analysis.

is listed in (Pan, 2012). We assume that layer 1 and layer 3 have the same elastic properties for computational convenience.

We have:

$$
\begin{pmatrix} u_x^3 \\ v_z^3 \\ \sigma_{zz}^3 \\ \tau_{zx}^3 \end{pmatrix} = \mathcal{C} \begin{pmatrix} u_x^1 \\ v_z^1 \\ \sigma_{zz}^1 \\ \tau_{zx}^1 \end{pmatrix} = \begin{pmatrix} C_{11} & C_{12} & C_{13} & C_{14} \\ C_{21} & C_{22} & C_{23} & C_{24} \\ C_{31} & C_{32} & C_{33} & C_{34} \\ C_{41} & C_{42} & C_{43} & C_{44} \end{pmatrix} \begin{pmatrix} u_x^1 \\ v_z^1 \\ \sigma_{zz}^1 \\ \tau_{zx}^1 \end{pmatrix} \tag{1}
$$

where $u_x^1, v_z^1, \sigma_{zz}^1, \tau_{zx}^1, u_x^3, v_z^3, \sigma_{zz}^3$ and τ_{zx}^3 represent the displacements and stresses in layers 1 and 3 respectively. Using these quantities we obtain:

$$
\mathcal{V}\mathcal{R} = \mathcal{X}, \tag{2}
$$

where $\mathcal{R} = \begin{pmatrix} R_{PP} & R_{PS} & T_{PP} & T_{PS} \end{pmatrix}^T, \mathcal{V} = \begin{pmatrix} \mathcal{V}_1 & \mathcal{V}_2 & \mathcal{V}_3 & \mathcal{V}_4 \end{pmatrix}$. And matrix $\mathcal{X}$ and each column in matrix $\mathcal{V}$ can be expressed using matrix $\mathcal{C}$ (Pan, 2012).

According to Cramer's rule, we can obtain four matrices $\mathcal{V}_{PP}, \mathcal{V}_{PS}, \mathcal{V}'_{PP}, \mathcal{V}'_{PS}$, by replacing the first, the second, the third and then the fourth columns of matrix $\mathcal{V}$ with $\mathcal{X}$. The elements of $\mathcal{X}$ and $\mathcal{V}$ are listed in Appendix A of Pan and Innanen (2013). We then express reflection and transmission coefficients as follows (e.g., Keys, 1989):

$$
R_{PP}(\theta, \omega, z) = \frac{det\mathcal{V}_{PP}}{det\mathcal{V}}, R_{PS}(\theta, \omega, z) = \frac{det\mathcal{V}_{PS}}{det\mathcal{V}}, T_{PP}(\theta, \omega, z) = \frac{det\mathcal{V}'_{PP}}{det\mathcal{V}}, T_{PS}(\theta, \omega, z) = \frac{det\mathcal{V}'_{PS}}{det\mathcal{V}}
$$
$$\tag{3}$$

where $det\{\cdot\}$ mean the determinant of the matrix.

AMPLITUDE RESPONSE IN ANELASTIC MEDIA

In this report, we continue our research of thin-bed AVO by taking attenuation into consideration in a dispersion system. Standard NCQ models (Aki and Richards, 2002; Innanen, 2012) are framed in terms of the propagation constants:

$$k_P = \frac{\omega}{V_P}[1 + Q_P^{-1}F_P(\omega)], k_S = \frac{\omega}{V_S}[1 + Q_S^{-1}F_S(\omega)], \tag{4}$$

where following "anacoustic" scattering theory (Innanen and Weglein, 2007) we have sequestered the attenuation and dispersion terms in the functions:

$$F_P(\omega) = \frac{i}{2} - \frac{1}{\pi}\log\left(\frac{\omega}{\omega_P}\right), F_S(\omega) = \frac{i}{2} - \frac{1}{\pi}\log\left(\frac{\omega}{\omega_S}\right), \tag{5}$$

equation (4) imply:

$$\tilde{V}_P = V_P[1 + Q_P^{-1}F_P(\omega)]^{-1}, \tilde{V}_S = V_P[1 + Q_S^{-1}F_S(\omega)]^{-1}, \tag{6}$$

Table.1 shows the elastic parameters used for amplitude response analysis. Layer 1 and Layer 3 are both shale with the same elastic parameters and Layer 2 indicating thin-bed is gas sand. Firstly, we fixed the thin-bed thickness z at $\frac{\lambda}{4}$ ($n = 4$) and fixed Q at 10, while varied the frequency from $10Hz$ to $80Hz$ with a step of $10Hz$. The Real parts of the R_{PP} and R_{PS} AVO curves are shown Fig.3a and b respectively. The black, red, blue, green, cyan, brown, pink and gray lines indicate the AVO curves when the frequency f is $10Hz$, $20Hz$, $30Hz$, $40Hz$, $50Hz$,$60Hz$, $70Hz$ and $80Hz$ respectively. And the bold black lines are the AVO curves without attenuation. We can observe that the R_{PP} AVO curves depart the AVO curve without attenuation with increasing frequency, while R_{PS} AVO curves approach the AVO curve without attenuation.

Then, we compared the Real parts of P-P reflections and P-S reflections with changing Q ($Q = Q_P = Q_S$) among $10, 20, 30, 40, 50$ and 90 indicated by magenta, red, blue, green, cyan, black lines and varying the thin-bed thickness among $n = 4$ (Fig.4), $n = 8$ (Fig.5), $n = 10$ (Fig.6), $n = 20$ (Fig.7), $n = 40$ (Fig.8), $n = 60$ (Fig.9), $n = 80$ (Fig.10) and $n = 100$ (Fig.11). We can see that with increasing Q the Real parts of the P-P reflection coefficients and P-S reflection coefficients approach the P-P reflections with no attenuation (the bold-black lines) as expected. Another thing we can observe is that with the thin-bed thinning, the influence of the Q increases for both R_{PP} and R_{PS}.

We also analyzed the influence of Q in the Imaginary parts of the R_{PP} and R_{PS}, as presented from Fig.12 to Fig.18 with decreasing the thin-bed thickness from $n = 4$ to $n = 80$. It can be seen that the influence of Q on Imaginary parts of R_{PP} and R_{PS} are small than that of Real parts of R_{PP} and R_{PS}.

LINEAR APPROXIMATION ANALYSIS

Ω and Λ coupled in matrix $\mathcal{C}$ (Pan, 2012; Pan and Innanen, 2013) are the P-wave wavenumber multiplied by thin-bed thickness z and S-wave wavenumber multiplied by the thin-bed thickness z, as listed in equation (7).

$$\Omega = \frac{\omega z}{\alpha_2}\cos\theta_2, \Lambda = \frac{\omega z}{\beta_2}\cos\gamma_2 \tag{7}$$

Table1. Elastic Model Parameters (gas bearing thin bed model)

Model	Rock Type	$\alpha(m/s)$	$\beta(m/s)$	α/β	$\rho(g/cm^3)$	σ
Layer 1	Shale	2850	1053	2.23	2.2	0.1
Layer 2	Gas sand	2900	1933	1.67	2.3	0.4
Layer 3	Shale	2850	1053	2.23	2.2	0.1
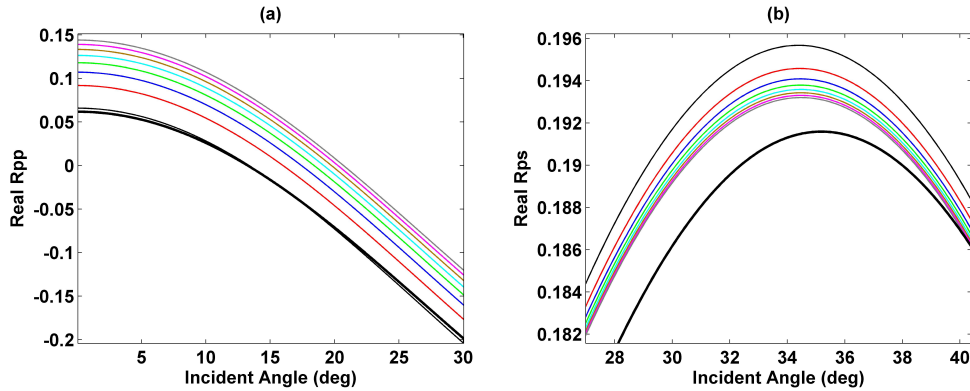
FIG. 3. Real R_{PP} (a) and R_{PS} (b) when $n = 4$ and $Q = 10$ while varying frequency from $10Hz$ to $80Hz$ with a step of $10Hz$.
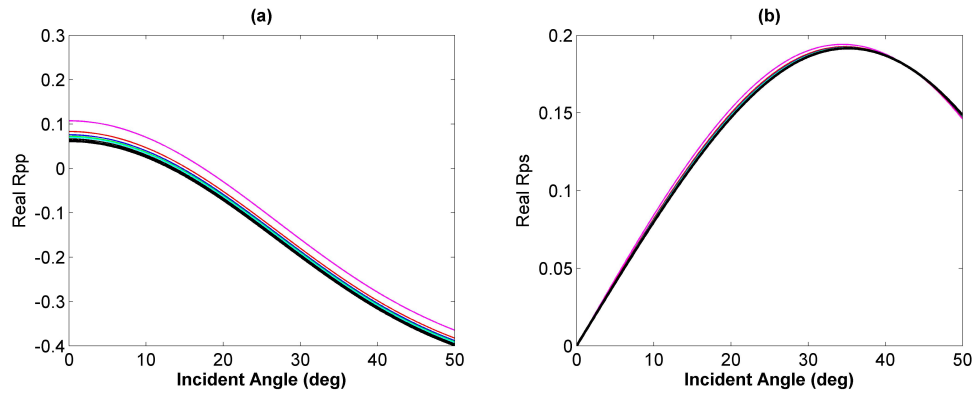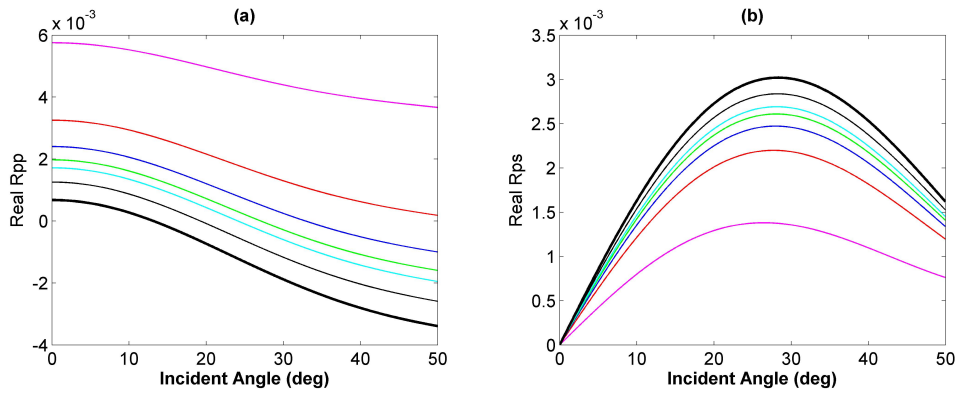

FIG. 4. Real R_{PP} (a) and R_{PS} (b) when $n = 4$ and frequency $f = 30Hz$.
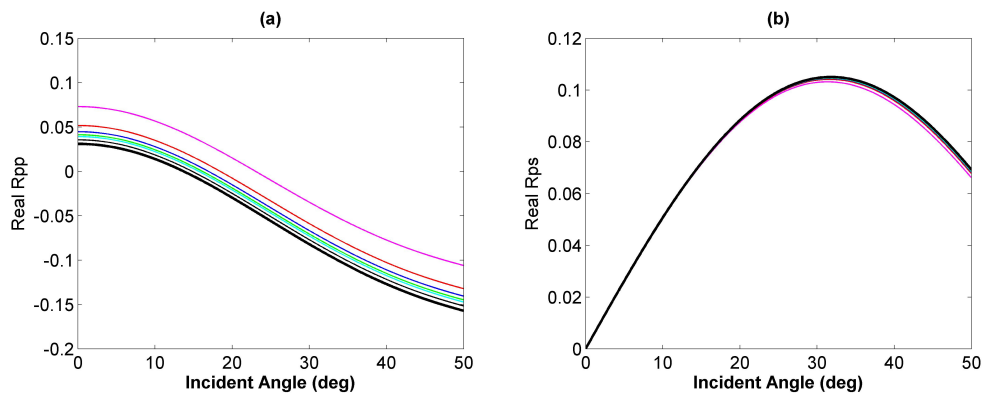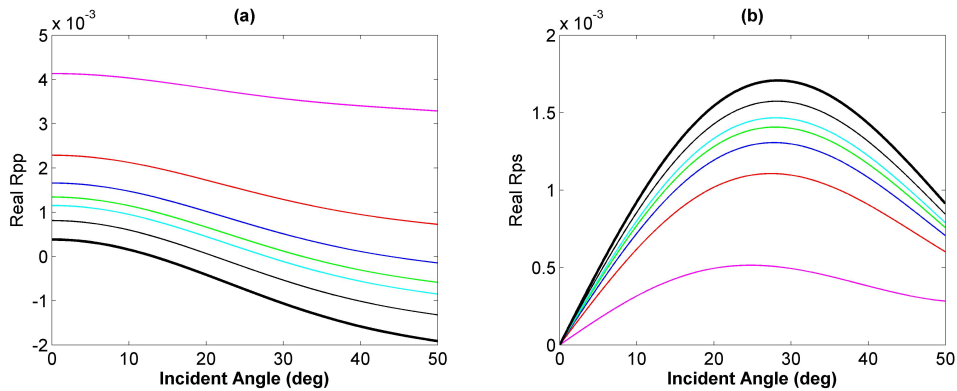

FIG. 5. Real R_{PP} (a) and R_{PS} (b) when $n = 8$ and frequency $f = 30Hz$.
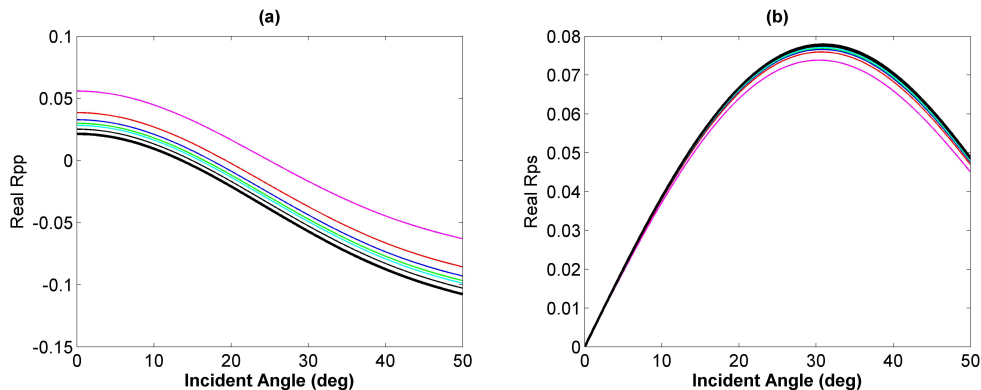
FIG. 6. Real R_{PP} (a) and R_{PS} (b) when $n = 10$ and frequency $f = 30Hz$.
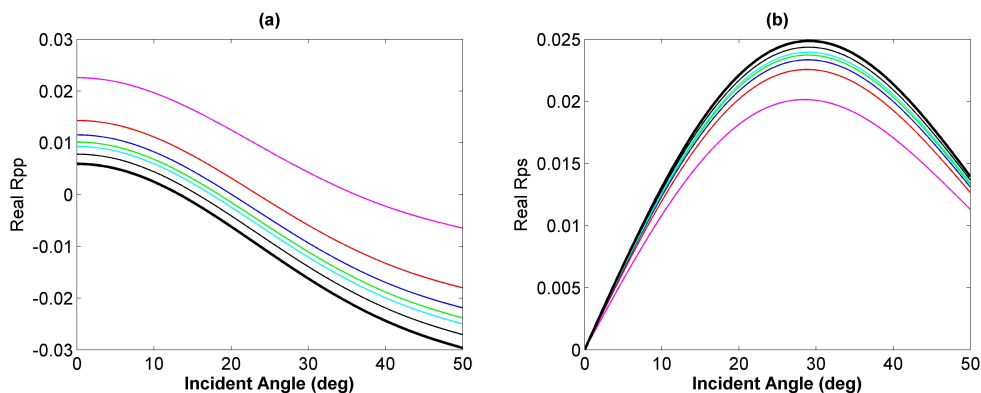
FIG. 7. Real R_{PP} (a) and R_{PS} (b) when $n = 20$ and frequency $f = 30Hz$.
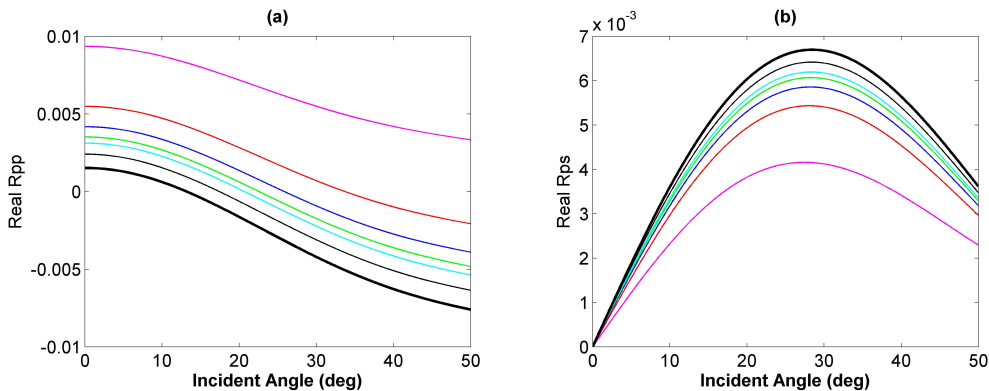
FIG. 8. Real R_{PP} (a) and R_{PS} (b) when $n = 40$ and frequency $f = 30Hz$.

Under the assumption that the thin-bed is ultra-thin, we simplified $\sin \Omega$, $\sin \Lambda \cos \Omega$ and $\cos \Lambda$ following Liu and Schmitt (2003)'s method. In this condition, they can be written as:

$$\sin \mathbf{\Omega} \simeq \mathbf{\Omega}, \sin \mathbf{\Lambda} \simeq \mathbf{\Lambda}, \tag{8}$$

$$\cos \mathbf{\Omega} \simeq 1, \cos \mathbf{\Lambda} \simeq 1.$$

Fig.19 shows the comparison between approximations and exact values for Absolute R_{PP} (Fig.19a) and R_{PS} (Fig.19b) when $n = 2$, $n = 6$, $n = 10$ and $n = 50$. The solid lines and cycle lines indicate the exact values and approximations respectively. It is obvious that with

FIG. 9. Real R_{PP} (a) and R_{PS} (b) when $n = 60$ and frequency $f = 30Hz$.

FIG. 10. Real R_{PP} (a) and R_{PS} (b) when $n = 80$ and frequency $f = 30Hz$.
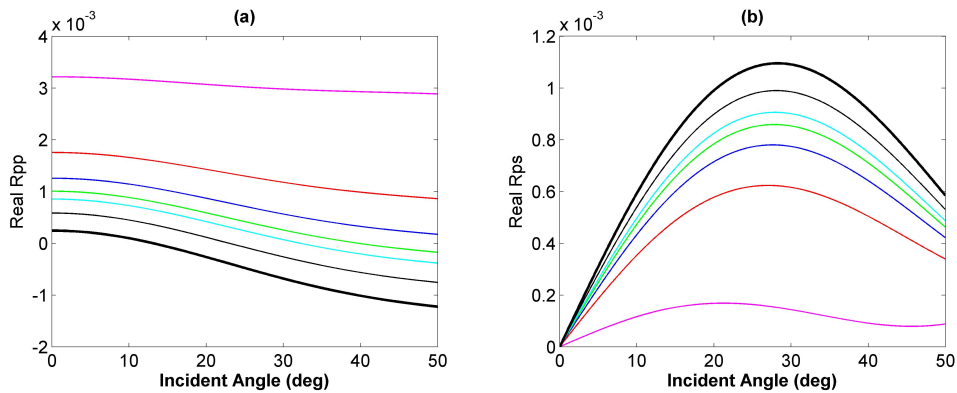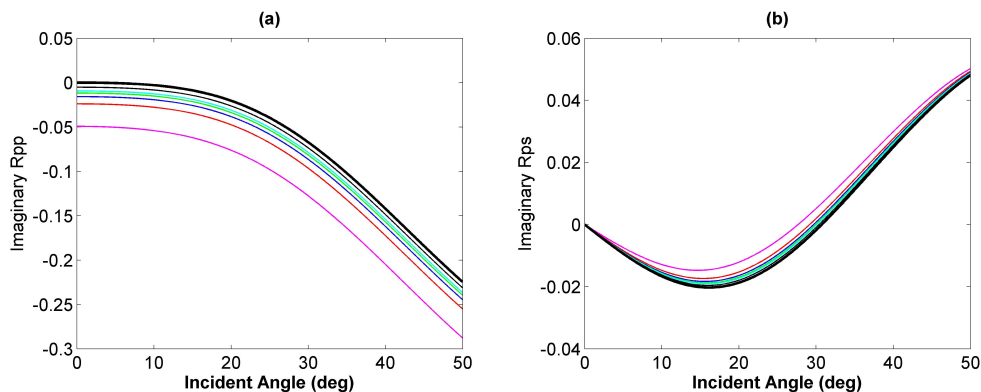

FIG. 11. Real R_{PP} (a) and R_{PS} (b) when $n = 100$ and frequency $f = 30Hz$.

the thin-bed thinning, the errors between the exact values and approximations are smaller for R_{PP} and R_{PS}. And we can also recognize that the errors for R_{PP} are smaller than that of R_{PS}.

NUMERICAL MODELING VERIFICATION

We built a 2D velocity model for numerical modeling, as shown by Fig.20. The whole model is $4000m$ in width and $3000m$ in depth. The top surface of the thin-bed is located at $1500m$ and the thin-bed thickness z can be $20m$ or $50m$. One single source is located at

FIG. 12. Imaginary R_{PP} (a) and R_{PS} (b) when $n = 4$ and frequency $f = 30Hz$.
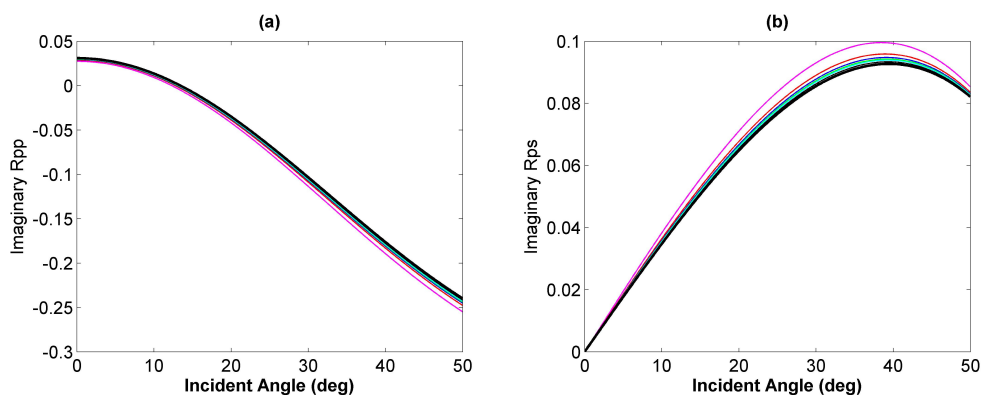

FIG. 13. Imaginary R_{PP} (a) and R_{PS} (b) when $n = 8$ and frequency $f = 30Hz$.

$[2000m, 0m]$ and 81 receivers are distributed at $1300m$ in depth with a spacing of $50m$. The source function is Ricker wavelet with a dominant frequency of $30Hz$. The boundaries of the model are set as absorbing boundary conditions. The elastic parameters of three layers in this model are consistent with those listed in Table.1.

Fig. 21a and b shows the seismic shot records when thin-bed thickness $z = 20m$ and $z = 50m$ respectively. We can notice that the reflections from the top interface and bottom interface of thin-bed can not be recognized and they are stacked together. We picked the P-P reflection amplitudes, as indicate by the red lines in Fig.21. Then we plotted the amplitudes obtained from numerical modeling and those obtained from our method for comparison, as presented in Fig.22.

The blue dash lines in Fig.22 indicate the P-P reflection R_{PP} obtained from numerical modeling, the blue dash lines are the AVO curves calculated by our method, and the black dash lines the AVO curves calculated by Zoeppritz equation. It can be seen that the AVO curves obtained by our method match those obtained from numerical modeling very well, which proves the correctness of our method.
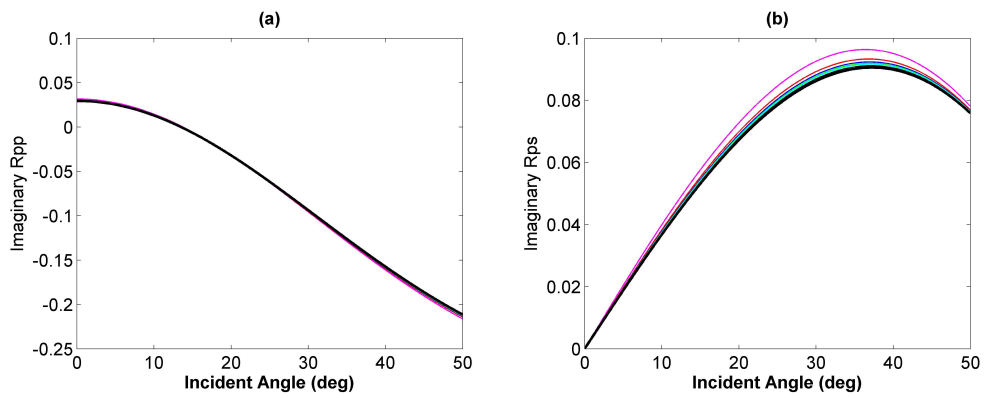
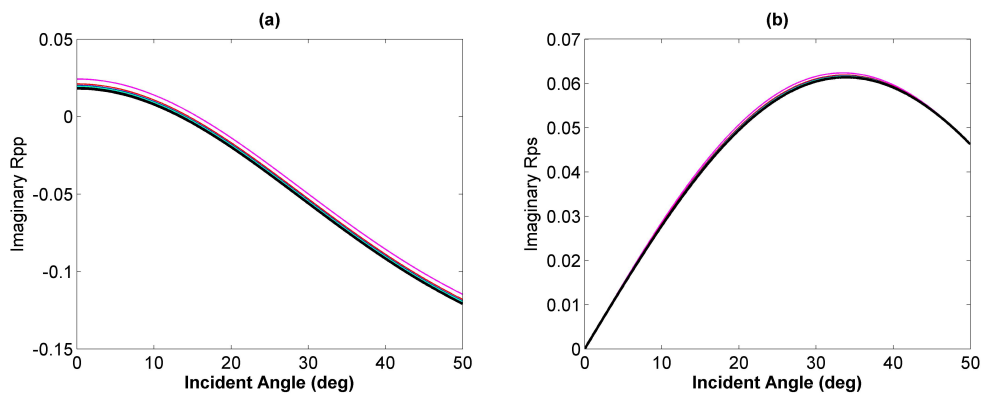FIG. 14. Imaginary R_{PP} (a) and R_{PS} (b) when $n = 10$ and frequency $f = 30Hz$.

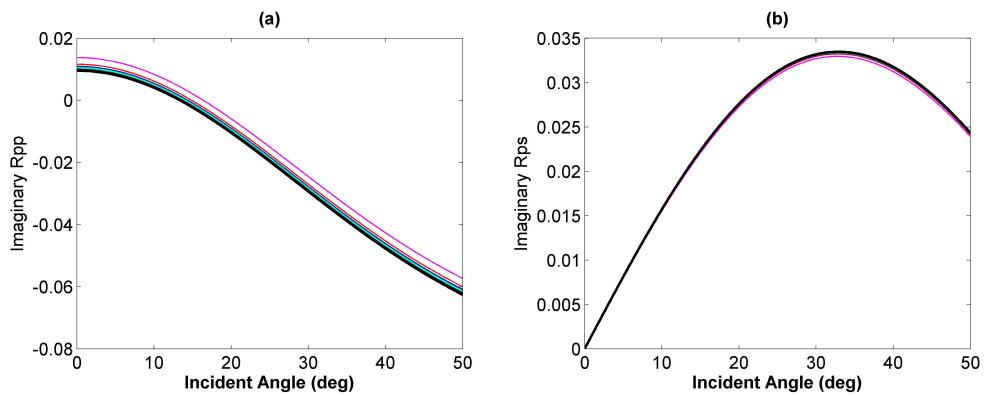FIG. 15. Imaginary R_{PP} (a) and R_{PS} (b) when $n = 20$ and frequency $f = 30Hz$.

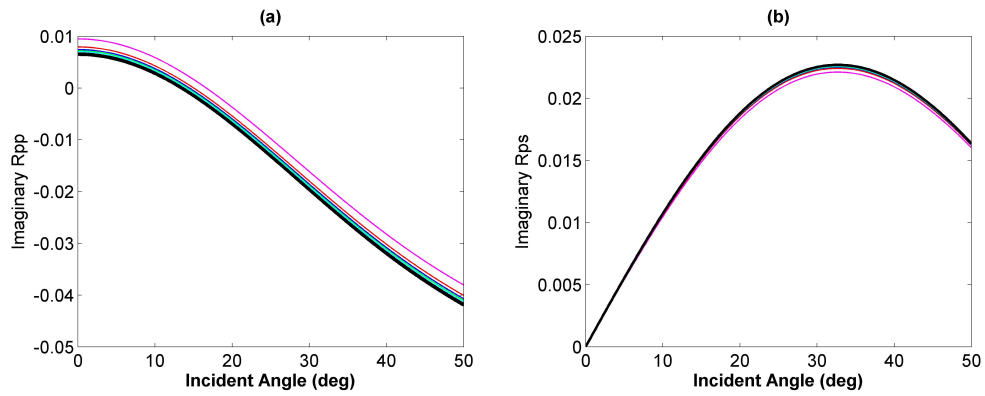FIG. 16. Imaginary R_{PP} (a) and R_{PS} (b) when $n = 40$ and frequency $f = 30Hz$.

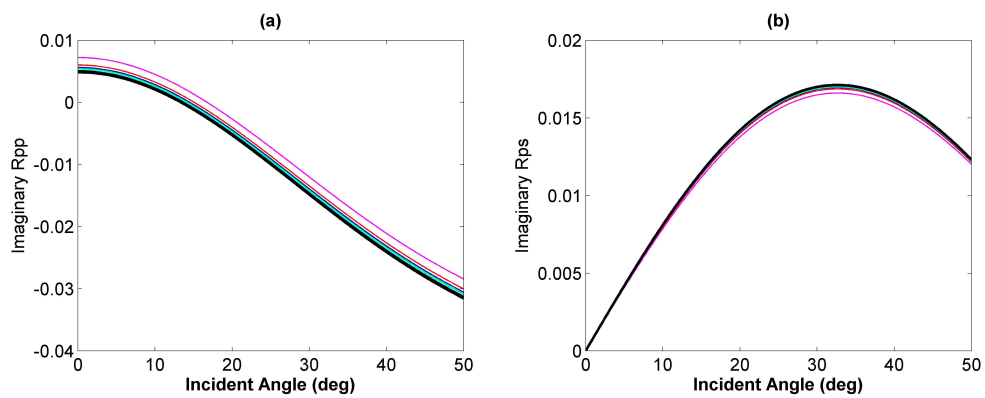FIG. 17. Imaginary R_{PP} (a) and R_{PS} (b) when $n = 60$ and frequency $f = 30Hz$.

FIG. 18. Imaginary R_{PP} (a) and R_{PS} (b) when $n = 80$ and frequency $f = 30Hz$.
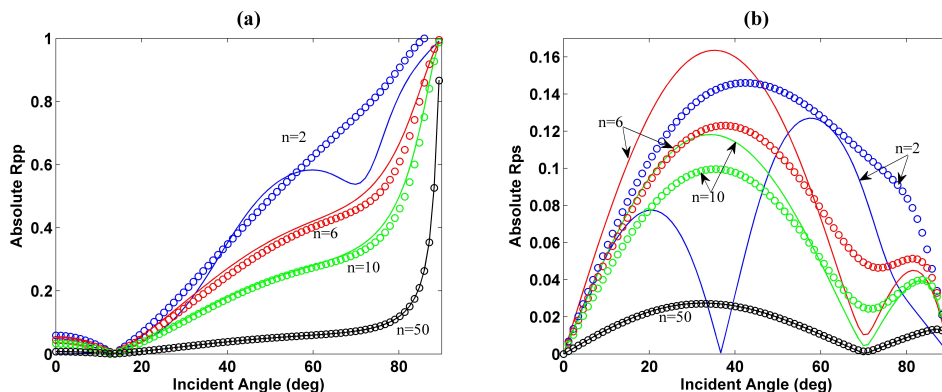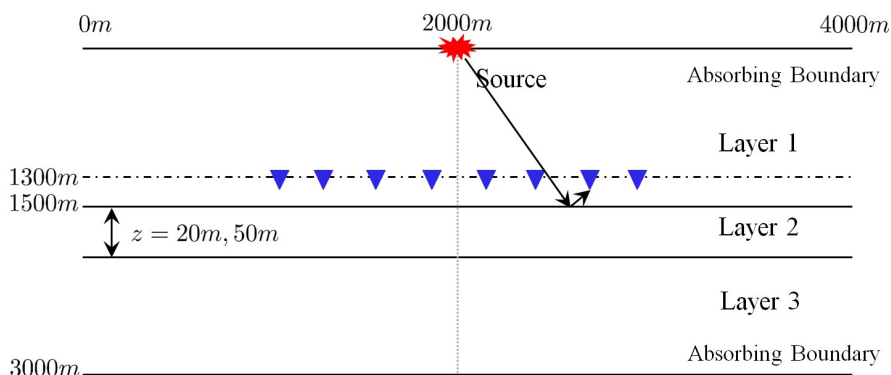
FIG. 19. Linear approximation analysis.

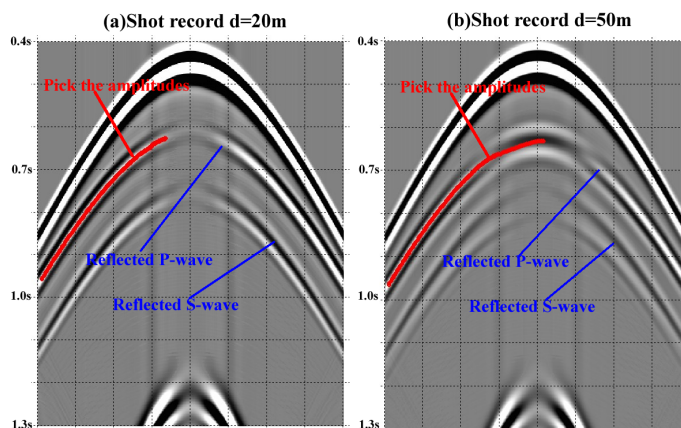FIG. 20. Geometry for numerical nodeling.

FIG. 21. Seismic shot records when thin-bed thickness $z = 20m$ (a) and $z = 50m$ (b) respectively.

CONCLUSION

Through the analysis and discussions above, we can achieve several conclusions: (1)If the thin-bed thickness and Q are both fixed, with increasing frequency, the Real part of R_{PP} AVO curve departs that with no attenuation, while the Real part of R_{PS} AVO curve approaches that without attenuation. (2) What's more, the influence of Q on Real parts of the reflections increases with thin-bed thinning. (3) With thin-bed thinning, the approxima-
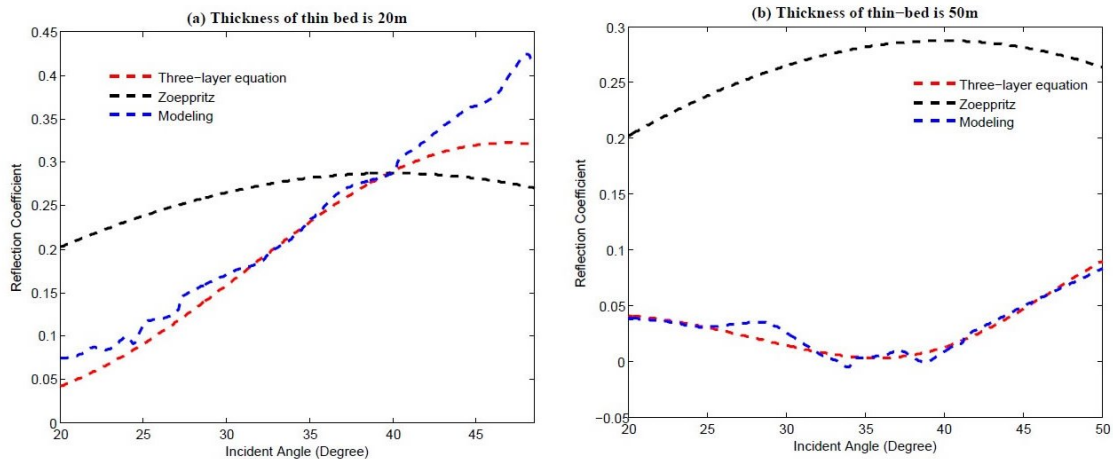
FIG. 22. P-P reflections R_{PP} comparison among numerical modeling results (blue dash line), our method (red dash line) and Zoeppritz equation (black dash line) when $z = 20m$ (a) and $z = 50m$ (b) respectively.

tions approach the exact values better. (4) The consistency between the amplitudes obtained from numerical modeling and that calculated by our method proves the correctness of our method.

ACKNOWLEDGEMENTS

REFERENCES

Aki, K., and Richards, P. G., 2002, Quantitative Seismology: University Science Books.

Brekhovskikh, L. M., 1993, Wave in layered media: Academic Press.

Innanen, K. A., 2012, Potentials for anelastic scattering: CREWES Report, **24**, 1–16.

Innanen, K. A., and Weglein, A. B., 2007, On the construction of an absorptive-dispersive medium model via direct linear inversion of reflected seismic primaries: Inverse Problems, **23**, 2289–2310.

Keys, R. G., 1989, Polarity reversals in reflections from layered media: Geophysics, **54**, 900–905.

Liu, Y., and Schmitt, D. R., 2003, Amplitude and avo responses of a single thin bed: Geophysics, **68**, 1161–1168.

Pan, W., 2012, Avo analysis for a single thin bed using three-layer media equation: CREWES Report, **24**, 1–23.

Pan, W., and Innanen, K. A., 2013, Avo/avf analysis of thin beds in elastic media, 373–377.